

# Physical Bounds and Optimal Currents on Antennas

Gustafsson, Mats; Cismasu, Marius; Jonsson, Lars

2011

CODEN:LUTEDX/(TEAT-7210)/1-22/(2011)

# Physical Bounds and Optimal Currents on Antennas

**Mats Gustafsson, Marius Cismasu, and B.L.G. Jonsson**

Electromagnetic Theory
Department of Electrical and Information Technology
Lund University
Sweden

Mats Gustafsson, Marius Cismasu
{Mats.Gustafsson,Marius.Cismasu}@eit.lth.se

Department of Electrical and Information Technology
Electromagnetic Theory
Lund University
P.O. Box 118
SE-221 00 Lund
Sweden

B. L. G. Jonsson
lars.jonsson@ee.kth.se

Electromagnetic Engineering Lab
School of Electrical Engineering
Royal Institute of Technology
Teknikringen 33
SE-100 44 Stockholm
Sweden

Editor: Gerhard Kristensson

**Abstract**

Physical bounds on the directivity Q-factor quotient and optimal current distributions are determined for antennas of arbitrary shape and size using an optimization formulation. A variational approach offers closed form solutions for small antennas expressed in the polarizability of the antenna structure. Finite sized antennas are solved using Lagrangian parameters in a method of moments formulation. It is also shown that the considered stored electric energy can be negative for electrically large objects. This effect is mitigated by a Helmholtz decomposition of the current density. Moreover, it is shown that the optimal charge density for a small antenna can be generated by several current densities. Numerical examples for small and large antennas are used to illustrate the results.

# 1 Introduction

Chu used spherical waves to express the stored and radiated energies outside the smallest circumscribing sphere of an antenna structure [4]. This approach has dominated the research on small antennas and offers many results on the Q-factor, and the directivity Q-factor quotient, $D/Q$, see [21] for an overview. The physical bounds on $D/Q$ were generalized to arbitrary shapes using the forward scattering sum rule in [6, 8, 9]. Yaghjian and Stuart derived bounds on the Q-factor in the limit of small antennas $ka \ll 1$, see [23]. In [20], Vandenbosch determines analogous bounds on $Q$ for non-magnetic antennas. The results in [6, 8, 9, 20, 23] are similar for the case of small dipole antennas composed of non-magnetic materials.

In this paper, new bounds on $D/Q$ are derived using the expression for the stored energy given by Geyi [5] for small antennas and generalized to finite size by Vandenbosch [19]. Closed form solutions are presented in the limit of small antennas, where it is shown that it is sufficient to consider surface currents and the minimization problem separates for electric dipoles, magnetic dipoles and their combinations. Moreover, the bounds for the electric dipole case are identical to the bounds in [6, 8, 9], in this limit. The combined bound also resembles the combined TE and TM bound by Thal [17] for spherical geometries.

Antennas are often considered as small if $ka \leq 1$ or $ka \leq 1/2$, which is a range of many interesting antennas. It is, hence, important to analyze the antenna performance for $ka$ in this range. Here, a Lagrangian formulation is used to solve the $D/Q$ optimization problem for finite $ka$. We show that this maximization problem has large similarities with solving the classical integral equations in electromagnetics using the method of moments (MoM). The maximizing currents are obtained by solving a linear system. This makes the approach attractive as it determines the optimal current distribution as well as the upper bounds on $D/Q$.

The expressions for the stored energies in [19] are very useful and produce similar bounds as in [6, 8, 9]. However, it is illustrated that the stored electric energy can be indefinite and explicit results are presented for divergence free loop type currents that have a negative stored electric energy for objects of the size $ka \approx 3/2$. It is

shown that this problem can be mitigated by a Helmholtz decomposition of the current.

The theoretical results are illustrated by numerical examples. The spherical region is used to illustrate that there are several optimal current densities that have identical charge densities. The considered current densities are similar to the current densities on folded spherical dipoles, capped spherical dipoles [16], and folded spherical helix [3] antennas. Planar structures are analyzed in detail and the obtained bounds are similar to the bounds in [6, 8–10, 12]. It is shown that the self-resonant strip dipole antenna has a current density that is close to the optimal current density and also performs close to the bound. Moreover, numerical simulations show that an array of capacitively loaded dipoles performs close to the bound.

This paper is organized as follows. The optimization formulation for $D/Q$ in the current density is introduced in Sec. 2. Closed form solutions in the limit of small antennas are derived using a variational formulation in Sec. 3. In Sec. 4, the $D/Q$ bound is solved with a Lagrangian formulation for finite size antennas. In Sec. 5, explicit examples are given that illustrates that the considered stored electric energy is negative for some divergence free loop type currents. Numerical examples for a spherical region, strip dipole antennas and two dipole arrays are presented in Sec. 6. Sec. 7 contains the conclusions.

# 2 Physical Bounds on the Directivity Q-factor Quotient

We consider antennas that are confined to a bounded volume $V$, see Fig. 1. It is assumed that the antenna structure is composed of non-magnetic materials. The electromagnetic fields are generated by the current densities, $\boldsymbol{J}$, flowing on the antenna.

To determine the directivity Q-factor quotient, $D/Q$, we express these quantities in terms of the definitions [2]. The partial directivity, $D(\hat{\boldsymbol{k}}, \hat{\boldsymbol{e}})$, characterizes the radiation properties of the antenna. It is defined as

$$D(\hat{\boldsymbol{k}}, \hat{\boldsymbol{e}}) = 4\pi \frac{P(\hat{\boldsymbol{k}}, \hat{\boldsymbol{e}})}{P_{\text{rad}}}, \tag{2.1}$$

where $P(\hat{\boldsymbol{k}}, \hat{\boldsymbol{e}})$ denotes the radiation intensity in the direction $\hat{\boldsymbol{k}}$ with polarization $\hat{\boldsymbol{e}}$ and $P_{\text{rad}}$ is the total radiated power. The quality factor, $Q$, is defined as

$$Q = \frac{2\omega W}{P_{\text{rad}}} = \frac{2\mathrm{c}_0 k W}{P_{\text{rad}}}, \tag{2.2}$$

where $W = \max\{W_{\text{e}}, W_{\text{m}}\}$ denotes the maximum of the stored electric and magnetic energies, $\omega$ is the angular frequency, $k$ the wavenumber, and $\mathrm{c}_0$ the speed of light in free space. Combine (2.1) and (2.2) to express the directivity Q-factor quotient as

$$\frac{D(\hat{\boldsymbol{k}}, \hat{\boldsymbol{e}})}{Q} = \frac{2\pi P(\hat{\boldsymbol{k}}, \hat{\boldsymbol{e}})}{\mathrm{c}_0 k W}. \tag{2.3}$$

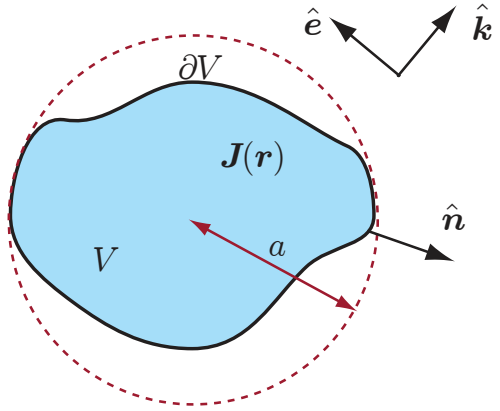


**Figure 1**: Illustration of the object geometry $V$, with boundary $\partial V$ and with outward normal unit vector $\hat{\boldsymbol{n}}$ and current density $\boldsymbol{J}(\boldsymbol{r})$. The radiated far field is evaluated in the $\hat{\boldsymbol{k}}$-direction for the polarization $\hat{\boldsymbol{e}}$ in free space. The object is circumscribed by a sphere with radius $a$.

We now express $D/Q$ in terms of the electric current density $\boldsymbol{J}$ in the antenna volume $V$. Note that there are no magnetic currents due to the assumption of non-magnetic materials. The radiation intensity from the current density $\boldsymbol{J}$ in the direction $\hat{\boldsymbol{k}}$ and polarization $\hat{\boldsymbol{e}}$ is

$$P(\hat{\boldsymbol{k}}, \hat{\boldsymbol{e}}) = \frac{\zeta_0 k^2}{32\pi^2} \left| \int_V \hat{\boldsymbol{e}}^* \cdot \boldsymbol{J}(\boldsymbol{r}) \mathrm{e}^{\mathrm{j}k\hat{\boldsymbol{k}}\cdot\boldsymbol{r}} \,\mathrm{d}V \right|^2, \tag{2.4}$$

where $\hat{\boldsymbol{k}} \cdot \hat{\boldsymbol{e}} = 0$ is used, $\zeta_0$ denotes the free space impedance, the superscript, $*$, denotes the complex conjugate, and the time convention $\mathrm{e}^{\mathrm{j}\omega t}$ is used.

The aim of this paper is to determine an upper bound on $D/Q$. It is not clear how to decompose the energy in its radiated and stored parts, see *e.g.*, [4, 5, 19, 24]. Similarly to the discussion in [20] we only use the vacuum terms of the stored energies, see also [22]. Here, we use the results by Vandenbosch [19], and write the free-space part of the stored electric energy as $\widetilde{W}_{\mathrm{vac}}^{(\mathrm{e})} = \frac{\mu_0}{16\pi k^2} w^{(\mathrm{e})}$, where

$$\begin{aligned} w^{(\mathrm{e})} = &\int_V \int_V \nabla_1 \cdot \boldsymbol{J}(\boldsymbol{r}_1) \nabla_2 \cdot \boldsymbol{J}^*(\boldsymbol{r}_2) \frac{\cos(k|\boldsymbol{r}_1 - \boldsymbol{r}_2|)}{|\boldsymbol{r}_1 - \boldsymbol{r}_2|} \\ &- \frac{k}{2} \big( k^2 \boldsymbol{J}(\boldsymbol{r}_1) \cdot \boldsymbol{J}^*(\boldsymbol{r}_2) - \nabla_1 \cdot \boldsymbol{J}(\boldsymbol{r}_1) \nabla_2 \cdot \boldsymbol{J}^*(\boldsymbol{r}_2) \big) \sin(k|\boldsymbol{r}_1 - \boldsymbol{r}_2|) \,\mathrm{d}V_1 \,\mathrm{d}V_2, \end{aligned} \tag{2.5}$$

and $\mu_0$ is the permeability of free space. The corresponding magnetic energy is $\widetilde{W}_{\mathrm{vac}}^{(\mathrm{m})} = \frac{\mu_0}{16\pi k^2} w^{(\mathrm{m})}$, where

$$\begin{aligned} w^{(\mathrm{m})} = &\int_V \int_V k^2 \boldsymbol{J}(\boldsymbol{r}_1) \cdot \boldsymbol{J}^*(\boldsymbol{r}_2) \frac{\cos(k|\boldsymbol{r}_1 - \boldsymbol{r}_2|)}{|\boldsymbol{r}_1 - \boldsymbol{r}_2|} \\ &- \frac{k}{2} \big( k^2 \boldsymbol{J}(\boldsymbol{r}_1) \cdot \boldsymbol{J}^*(\boldsymbol{r}_2) - \nabla_1 \cdot \boldsymbol{J}(\boldsymbol{r}_1) \nabla_2 \cdot \boldsymbol{J}^*(\boldsymbol{r}_2) \big) \sin(k|\boldsymbol{r}_1 - \boldsymbol{r}_2|) \,\mathrm{d}V_1 \,\mathrm{d}V_2. \end{aligned} \tag{2.6}$$

We now have an explicit expression for $D/Q$ in the current density $\boldsymbol{J}$, *i.e.*,

$$\frac{D(\hat{\boldsymbol{k}},\hat{\boldsymbol{e}})}{Q} = k^3 \frac{\left|\int_V \hat{\boldsymbol{e}}^* \cdot \boldsymbol{J}(\boldsymbol{r}) \mathrm{e}^{\mathrm{j}k\hat{\boldsymbol{k}}\cdot\boldsymbol{r}} \,\mathrm{dV}\right|^2}{\max\{w^{(\mathrm{e})}(\boldsymbol{J}), w^{(\mathrm{m})}(\boldsymbol{J})\}}, \tag{2.7}$$

where $w^{(\mathrm{e})}(\boldsymbol{J})$ and $w^{(\mathrm{m})}(\boldsymbol{J})$ are defined in (2.5) and (2.6). The $D/Q$ quotient is maximized to produce physical bounds, *i.e.*,

$$\frac{D(\hat{\boldsymbol{k}},\hat{\boldsymbol{e}})}{Q} \leq \max_{\boldsymbol{J}} k^3 \frac{\left|\int_V \hat{\boldsymbol{e}}^* \cdot \boldsymbol{J}(\boldsymbol{r}) \mathrm{e}^{\mathrm{j}k\hat{\boldsymbol{k}}\cdot\boldsymbol{r}} \,\mathrm{dV}\right|^2}{\max\{w^{(\mathrm{e})}(\boldsymbol{J}), w^{(\mathrm{m})}(\boldsymbol{J})\}}, \tag{2.8}$$

where $\boldsymbol{J}$ are all the admissible current densities in $V$. The continuity of the normal component requires that $\hat{\boldsymbol{n}} \cdot \boldsymbol{J}(\boldsymbol{r}) = 0$ for $\boldsymbol{r} \in \partial V$, where $\hat{\boldsymbol{n}}$ is the outward unit normal of the antenna volume $V$, see Fig. 1.

Note that (2.8) is invariant for amplitude scalings $\boldsymbol{J} \to \alpha\boldsymbol{J}$, and if $\boldsymbol{J}_0$ is a solution to the maximization problem, then $\boldsymbol{J}_1 = \boldsymbol{J}_0 / \int \hat{\boldsymbol{e}}^* \cdot \boldsymbol{J}_0 \mathrm{e}^{\mathrm{j}k\hat{\boldsymbol{k}}\cdot\boldsymbol{r}} \,\mathrm{dV}$ is another solution to it. This property is used repeatedly in the upcoming sections to reformulate the optimization problem and to determine the maximizing current density.

We first analyze electrically small antennas to find closed form solutions of the $D/Q$-bound in Sec. 3, *i.e.*, the current expressions are analyzed in the limit $ka \to 0$, where $a$ denotes the radius of the smallest sphere that circumscribes the antenna volume $V$. The general case with finite $ka$ is considered in Sec. 4.

# 3 Electrically Small Antennas

The radiation intensity (2.4) and stored electric (2.5) and magnetic (2.6) energies simplify in the low-frequency limit, $k \to 0$ for fixed $a$. We use the expansions $\mathrm{e}^{\mathrm{j}k\hat{\boldsymbol{k}}\cdot\boldsymbol{r}} = 1 + \mathrm{j}k\hat{\boldsymbol{k}}\cdot\boldsymbol{r} + \mathcal{O}(k^2)$ and $\boldsymbol{J} = \boldsymbol{J}^{(0)} + k\boldsymbol{J}^{(1)} + o(k)$ as $k \to 0$, where $\nabla\cdot\boldsymbol{J}^{(0)} = 0$ and $\nabla\cdot\boldsymbol{J}^{(1)} = -\mathrm{j}\rho$ follow from the continuity equation. Note that the charge density in SI-units is given by $\rho_{\mathrm{SI}} = \rho/\mathrm{c}_0$. The radiation intensity (2.4) is expanded as

$$\begin{aligned}\int_V \boldsymbol{J}(\boldsymbol{r}) \mathrm{e}^{\mathrm{j}k\hat{\boldsymbol{k}}\cdot\boldsymbol{r}} \,\mathrm{dV} &= \int_V \boldsymbol{J}^{(0)}(\boldsymbol{r}) + k\boldsymbol{J}^{(1)}(\boldsymbol{r}) + \mathrm{j}k\hat{\boldsymbol{k}}\cdot\boldsymbol{r}\boldsymbol{J}^{(0)}(\boldsymbol{r}) + \mathcal{O}(k^2) \,\mathrm{dV} \\ &= -k\int_V \boldsymbol{r}\nabla\cdot\boldsymbol{J}^{(1)}(\boldsymbol{r}) + \frac{\mathrm{j}}{2}\hat{\boldsymbol{k}}\times(\boldsymbol{r}\times\boldsymbol{J}^{(0)}(\boldsymbol{r})) \,\mathrm{dV} + \mathcal{O}(k^2), \end{aligned} \tag{3.1}$$

as $k \to 0$, see [18]. We observe that the first term corresponds to an electric dipole and the second term to a magnetic dipole. The electric (2.5) and magnetic (2.6) energies have the low-frequency expansions [5, 19, 20]

$$w^{(\mathrm{e})} = k^2 \int_V \int_V \frac{\rho(\boldsymbol{r}_1)\rho^*(\boldsymbol{r}_2)}{|\boldsymbol{r}_1 - \boldsymbol{r}_2|} \,\mathrm{dV}_1 \,\mathrm{dV}_2 \tag{3.2}$$

and

$$w^{(\mathrm{m})} = k^2 \int_V \int_V \frac{\boldsymbol{J}^{(0)}(\boldsymbol{r}_1)\cdot\boldsymbol{J}^{(0)*}(\boldsymbol{r}_2)}{|\boldsymbol{r}_1 - \boldsymbol{r}_2|} \,\mathrm{dV}_1 \,\mathrm{dV}_2, \tag{3.3}$$

respectively. Insert the last three expressions into (2.8) to get the bound

$$\frac{D}{Q} \leq \max_{\rho, \boldsymbol{J}^{(0)}} \frac{k^3 \left| \int_V \hat{\boldsymbol{e}}^* \cdot \boldsymbol{r}\rho(\boldsymbol{r}) + \frac{1}{2}\hat{\boldsymbol{h}}^* \times \boldsymbol{r} \cdot \boldsymbol{J}^{(0)}(\boldsymbol{r}) \, \mathrm{d}V \right|^2}{\max\left\{ \iint_V \frac{\rho(\boldsymbol{r}_1)\rho^*(\boldsymbol{r}_2)}{|\boldsymbol{r}_1 - \boldsymbol{r}_2|} \, \mathrm{dV}_1 \, \mathrm{dV}_2, \int_V \int_V \frac{\boldsymbol{J}^{(0)}(\boldsymbol{r}_1) \cdot \boldsymbol{J}^{(0)*}(\boldsymbol{r}_2)}{|\boldsymbol{r}_1 - \boldsymbol{r}_2|} \, \mathrm{dV}_1 \, \mathrm{dV}_2 \right\}}, \tag{3.4}$$

where we have used the magnetic polarization $\hat{\boldsymbol{h}} = \hat{\boldsymbol{k}} \times \hat{\boldsymbol{e}}$. We observe that the optimization decouples in $\rho$ and $\boldsymbol{J}^{(0)}$, see App. A. The case with $\boldsymbol{J}^{(0)} = \boldsymbol{0}$ corresponds to an antenna radiating as an electric dipole and it is analyzed in Sec. 3.1. The case with $\rho = 0$ corresponds to an antenna radiating as a magnetic dipole and it is analyzed in Sec. 3.2. In general, both quantities can be non-zero and this case is discussed in Sec. 3.3.

## 3.1 Electric Dipole

A small antenna that radiates as an electric dipole, *i.e.*, $\boldsymbol{J}^{(0)} = \boldsymbol{0}$ in (3.4), gives the maximization problem:

$$\frac{D_\mathrm{e}}{Q_\mathrm{e}} \leq \max_{\rho} \frac{k^3}{4\pi} \frac{\left| \int \hat{\boldsymbol{e}}^* \cdot \boldsymbol{r}\rho(\boldsymbol{r}) \, \mathrm{d}V \right|^2}{\int_V \int_V \frac{\rho(\boldsymbol{r}_1)\rho^*(\boldsymbol{r}_2)}{4\pi|\boldsymbol{r}_1 - \boldsymbol{r}_2|} \, \mathrm{dV}_1 \, \mathrm{dV}_2}. \tag{3.5}$$

The term $4\pi$ is included to simplify the identification with the free-space Green's function.

Consider the optimization problem:

$$\max_{\rho} \frac{\left| \int \hat{\boldsymbol{e}}^* \cdot \boldsymbol{r}\rho(\boldsymbol{r}) \, \mathrm{d}V \right|^2}{\int_V \int_V \frac{\rho(\boldsymbol{r}_1)\rho^*(\boldsymbol{r}_2)}{4\pi|\boldsymbol{r}_1 - \boldsymbol{r}_2|} \, \mathrm{dV}_1 \, \mathrm{dV}_2}, \tag{3.6}$$

subject to the constraint $\int_V \rho \, \mathrm{dV} = -\mathrm{j} \int_{\partial V} \hat{\boldsymbol{n}} \cdot \boldsymbol{J}^{(1)} \, \mathrm{dS} = 0$ that follows from the continuity of the normal component of the current density, *i.e.*, $\hat{\boldsymbol{n}} \cdot \boldsymbol{J}^{(1)} = 0$ at the boundary. We note that this maximization problem is homogeneous for scalings $\rho \to \alpha\rho$ and, if $\rho_a$ is a solution to (3.6), then $\rho_b = \rho_a / \int \hat{\boldsymbol{e}}^* \cdot \boldsymbol{r}\rho_a \, \mathrm{dV}$ is another solution to it. Thus, (3.6) can be rewritten as

$$\min_{\rho} \int_V \int_V \frac{\rho(\boldsymbol{r}_1)\rho^*(\boldsymbol{r}_2)}{4\pi|\boldsymbol{r}_1 - \boldsymbol{r}_2|} \, \mathrm{dV}_1 \, \mathrm{dV}_2, \tag{3.7}$$

subject to the scaling invariant constraints $\int \hat{\boldsymbol{e}}^* \cdot \boldsymbol{r}\rho(\boldsymbol{r}) \, \mathrm{dV} = E_0\gamma$ and the charge conservation constraint $\int \rho(\boldsymbol{r}) \, \mathrm{dV} = 0$, where $E_0 \in \mathbb{C}$ and $\gamma \in \mathbb{R}$ are constants. This is a standard minimization problem that is easily solved by introducing basis functions for $\rho$ and using Lagrange multipliers [15]. We can also write the solution as an integral equation using a variational formulation. The minimum of (3.7) is stationary with respect to variations $\rho \to \rho + \delta\rho'$ as $\delta \to 0$. To the first order in $\delta$, we get

$$\int_V \rho'(\boldsymbol{r}_2) \int_V \frac{\rho^*(\boldsymbol{r}_1)}{4\pi|\boldsymbol{r}_1 - \boldsymbol{r}_2|} \, \mathrm{dV}_1 \, \mathrm{dV}_2 = 0, \tag{3.8}$$

together with

$$\int_V \hat{\boldsymbol{e}}^* \cdot \boldsymbol{r}\rho'(\boldsymbol{r})\,\mathrm{dV} = 0 \quad \text{and} \quad \int_V \rho'(\boldsymbol{r})\,\mathrm{dV} = 0, \tag{3.9}$$

for all $\rho'(\boldsymbol{r})$. This shows that $\rho$ satisfies the volume integral equation

$$\int_V \frac{\rho(\boldsymbol{r}_1)}{4\pi|\boldsymbol{r}_1 - \boldsymbol{r}_2|}\,\mathrm{dV}_1 = E_0\hat{\boldsymbol{e}} \cdot \boldsymbol{r}_2 + C \quad \text{for } \boldsymbol{r}_2 \in V, \tag{3.10}$$

where $E_0$ is the constant introduced above and the constant $C$ is determined from the condition $\int \rho(\boldsymbol{r})\,\mathrm{dV} = 0$. This is an integral equation for the region $V$ with constant potential and zero total charge in a homogeneous exterior electric field $E_0\hat{\boldsymbol{e}}$. Applying $\nabla^2$ to (3.10) shows that $\rho(\boldsymbol{r}_2) = 0$ for $\boldsymbol{r}_2 \in V \setminus \partial V$. The solution is hence given by the surface charge density $\rho_\mathrm{s}$, determined from the boundary integral equation

$$\int_{\partial V} \frac{\rho_\mathrm{s}(\boldsymbol{r}_1)}{4\pi|\boldsymbol{r}_1 - \boldsymbol{r}_2|}\,\mathrm{dS}_1 = E_0\hat{\boldsymbol{e}} \cdot \boldsymbol{r}_2 + C \quad \text{for } \boldsymbol{r}_2 \in \partial V. \tag{3.11}$$

This is the integral equation for the charge density used in the computation of the high-contrast polarizability dyadics [13]. Rewriting (3.5) by making use of the previous results, we get

$$\frac{D_\mathrm{e}}{Q_\mathrm{e}} \leq \frac{k^3}{4\pi}\frac{|E_0|^2\gamma^2}{\int_{\partial V}\int_{\partial V}\frac{\rho_\mathrm{s}(\boldsymbol{r}_1)\rho_\mathrm{s}^*(\boldsymbol{r}_2)}{4\pi|\boldsymbol{r}_1-\boldsymbol{r}_2|}\,\mathrm{dS}_1\,\mathrm{dS}_2} = \frac{k^3}{4\pi}\gamma. \tag{3.12}$$

Using the high-contrast polarizability dyadic of the region $V$,

$$\gamma = \hat{\boldsymbol{e}}^* \cdot \boldsymbol{\gamma}_\infty \cdot \hat{\boldsymbol{e}} = \frac{1}{E_0}\int_{\partial V} \hat{\boldsymbol{e}}^* \cdot \boldsymbol{r}\rho_\mathrm{s}(\boldsymbol{r})\,\mathrm{dS}, \tag{3.13}$$

we obtain the final bound

$$\frac{D_\mathrm{e}(\hat{\boldsymbol{k}}, \hat{\boldsymbol{e}})}{Q_\mathrm{e}} \leq \frac{k^3}{4\pi}\hat{\boldsymbol{e}}^* \cdot \boldsymbol{\gamma}_\infty \cdot \hat{\boldsymbol{e}}. \tag{3.14}$$

The bound (3.12) is identical to the bound in [8, 9] for the generalized absorption efficiency $\eta = 1/2$. This verifies that $\eta = 1/2$ for small dipole antennas as shown in [6]. It is also observed that $\eta \approx 1/2$ for many narrow band, $Q \gg 1$, minimum scattering antennas , *i.e.*, it is not required that $ka \to 0$ for the bound in [8, 9] to hold.

The bound (3.14) is illustrated in Fig. 2 for a spheroid with height $\ell_\mathrm{z}$, width $\ell_\mathrm{x}$, and polarization $\hat{\boldsymbol{e}} = \hat{\boldsymbol{x}}$, see App. B for details[1]. It is observed that $D_\mathrm{e}/Q_\mathrm{e} \leq k^3a^3$ for a sphere $\ell_\mathrm{x} = \ell_\mathrm{z}$. This can also be written $Q_\mathrm{e} \geq 3/(2k^3a^3)$ as $D = 3/2$ for small dipole antennas. This is identical to the bound by Thal [17]. The bound approaches $D_\mathrm{e}/Q_\mathrm{e} \leq 4k^3a^3/(3\pi)$ and $Q_\mathrm{e} \geq 9\pi/(8k^3a^3)$ in the limit of a circular disc $\ell_\mathrm{z} = 0$, see also [8–10, 23].

[1] see also http://www.mathworks.com/matlabcentral/fileexchange/26806-antennaq

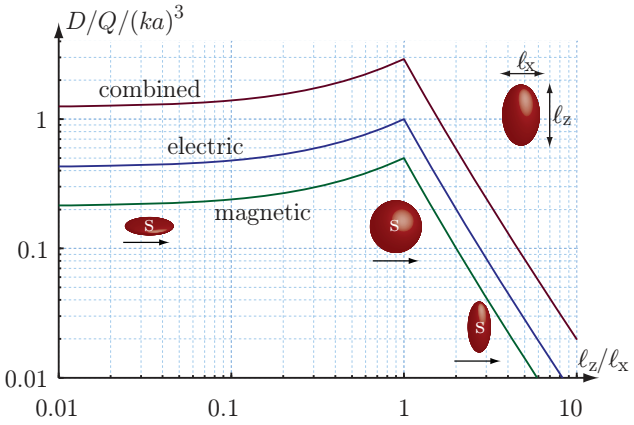


**Figure 2**: Bounds on $D/(Qk^3a^3)$ for a spheroid with height $\ell_z$, width $\ell_x$, electric polarization $\hat{\boldsymbol{e}} = \hat{\boldsymbol{x}}$, and $a = \max\{\ell_x, \ell_z\}/2$.

## 3.2 Magnetic Dipole

The corresponding magnetic dipole radiator is obtained when $\rho = 0$ in (3.4) and its $D/Q$ performance is bounded by

$$\frac{D_{\mathrm{m}}}{Q_{\mathrm{m}}} \leq \frac{k^3}{4\pi} \max_{\boldsymbol{J}^{(0)}} \frac{\left| \int_V \frac{1}{2} \hat{\boldsymbol{h}}^* \times \boldsymbol{r} \cdot \boldsymbol{J}^{(0)}(\boldsymbol{r}) \, \mathrm{d}V \right|^2}{\int_V \int_V \frac{\boldsymbol{J}^{(0)}(\boldsymbol{r}_1) \cdot \boldsymbol{J}^{(0)*}(\boldsymbol{r}_2)}{4\pi |\boldsymbol{r}_1 - \boldsymbol{r}_2|} \, \mathrm{d}V_1 \, \mathrm{d}V_2}, \tag{3.15}$$

where $\hat{\boldsymbol{h}} = \hat{\boldsymbol{k}} \times \hat{\boldsymbol{e}}$. We use the amplitude scaling invariance to rewrite the minimization problem as

$$\min_{\boldsymbol{J}^{(0)}} \int_V \int_V \frac{\boldsymbol{J}^{(0)}(\boldsymbol{r}_1) \cdot \boldsymbol{J}^{(0)*}(\boldsymbol{r}_2)}{4\pi |\boldsymbol{r}_1 - \boldsymbol{r}_2|} \, \mathrm{d}V_1 \, \mathrm{d}V_2, \tag{3.16}$$

subject to the constraints $\nabla \cdot \boldsymbol{J}^{(0)} = 0$ and $\frac{1}{2} \int_V \hat{\boldsymbol{h}}^* \times \boldsymbol{r} \cdot \boldsymbol{J}^{(0)}(\boldsymbol{r}) \, \mathrm{d}V = H_0 \nu$, where $H_0 \in \mathbb{C}$ and $\nu \in \mathbb{R}$ are constants. The perturbation $\boldsymbol{J}^{(0)} \to \boldsymbol{J}^{(0)} + \delta \boldsymbol{J}^{(0)'}$ shows that

$$\int_V \boldsymbol{J}^{(0)'}(\boldsymbol{r}_2) \cdot \int_V \frac{\boldsymbol{J}^{(0)*}(\boldsymbol{r}_1)}{4\pi |\boldsymbol{r}_1 - \boldsymbol{r}_2|} \, \mathrm{d}V_1 \, \mathrm{d}V_2 = 0, \tag{3.17}$$

$$\int_V \hat{\boldsymbol{h}}^* \times \boldsymbol{r} \cdot \boldsymbol{J}^{(0)'}(\boldsymbol{r}) \, \mathrm{d}V = 0, \tag{3.18}$$

and $\nabla \cdot \boldsymbol{J}^{(0)'} = 0$. Thus, the solution satisfies the following volume integral equation:

$$\int_V \frac{\boldsymbol{J}^{(0)}(\boldsymbol{r}_1)}{4\pi |\boldsymbol{r}_1 - \boldsymbol{r}_2|} \, \mathrm{d}V_1 = \frac{H_0}{2} \hat{\boldsymbol{h}} \times \boldsymbol{r}_2 + \nabla \psi(\boldsymbol{r}_2) \quad \text{for } \boldsymbol{r}_2 \in V, \tag{3.19}$$

where $\psi(\boldsymbol{r}_2)$ is an arbitrary function to account for the constraint $\nabla \cdot \boldsymbol{J}^{(0)} = 0$, assuming sufficient constraint on the regularity of the domain (*e.g.*, Lipschitz) and functions that Green's formula hold see *e.g.*, [14]. Taking the divergence of the

above equation and using $\hat{\boldsymbol{n}}(\boldsymbol{r}) \cdot \boldsymbol{J}^{(0)}(\boldsymbol{r}) = 0$ for $\boldsymbol{r} \in \partial V$, shows that $\nabla^2 \psi(\boldsymbol{r}_2) = 0$ for $\boldsymbol{r}_2 \in V$. Applying $\nabla \times \nabla \times \cdot$ to (3.19) implies that $\boldsymbol{J}^{(0)}(\boldsymbol{r}_2) = \boldsymbol{0}$ for $\boldsymbol{r}_2 \in V \setminus \partial V$. This gives the boundary integral equation for the surface current density $\boldsymbol{J}_{\mathrm{s}}^{(0)}(\boldsymbol{r}_1)$ as:

$$\hat{\boldsymbol{n}} \times \int_{\partial V} \frac{\boldsymbol{J}_{\mathrm{s}}^{(0)}(\boldsymbol{r}_1)}{4\pi |\boldsymbol{r}_1 - \boldsymbol{r}_2|} \, \mathrm{dS}_1 = \frac{H_0}{2} \hat{\boldsymbol{n}} \times (\hat{\boldsymbol{h}} \times \boldsymbol{r}_2) + \hat{\boldsymbol{n}} \times \nabla \psi(\boldsymbol{r}_2) \quad \text{for } \boldsymbol{r}_2 \in \partial V. \tag{3.20}$$

Note that the restrictions to the tangential components follow from the vanishing normal component of the current density at the boundary, *i.e.*, $\hat{\boldsymbol{n}} \cdot \boldsymbol{J}^{(0)'}(\boldsymbol{r}_2) = 0$ for $\boldsymbol{r}_2 \in \partial V$ in (3.17).

The bound for the optimizing $\boldsymbol{J}_{\mathrm{s}}$ (3.15) becomes

$$\frac{D_{\mathrm{m}}}{Q_{\mathrm{m}}} \leq \frac{k^3}{4\pi} \frac{|H_0|^2 \nu^2}{\int_{\partial V} \int_{\partial V} \frac{\boldsymbol{J}_{\mathrm{s}}^{(0)}(\boldsymbol{r}_1) \cdot \boldsymbol{J}_{\mathrm{s}}^{(0)*}(\boldsymbol{r}_2)}{4\pi |\boldsymbol{r}_1 - \boldsymbol{r}_2|} \, \mathrm{dS}_1 \, \mathrm{dS}_2} = \frac{k^3}{4\pi} \nu. \tag{3.21}$$

where we identify $\nu$ as the $\hat{\boldsymbol{h}}$-component of the magnetic moment.

The bound for a spheroid with $\hat{\boldsymbol{h}} = \hat{\boldsymbol{z}}$ and surface currents $\boldsymbol{J} = J_\phi \hat{\boldsymbol{\phi}}$ is depicted in Fig. 2. It is observed that $D_{\mathrm{m}}/Q_{\mathrm{m}} = D_{\mathrm{e}}/(2Q_{\mathrm{e}})$ for this case, see also App. B. In particular this gives $D_{\mathrm{m}}/Q_{\mathrm{m}} \leq k^3 a^3/2$ and $D_{\mathrm{m}}/Q_{\mathrm{m}} \leq k^3 a^3 8/3$ for spheres and discs, respectively.

## 3.3 Combined Electric and Magnetic Dipoles

Maximization of (3.4) is given by the combination of the electric and magnetic dipole cases. It is first observed that

$$\max_{a,b} \frac{|\alpha a + \beta b|^2}{\max\{|a|^2, |b|^2\}} = (\alpha + \beta)^2, \tag{3.22}$$

for $\alpha \geq 0$ and $\beta \geq 0$, see App. A. Replace $\alpha$ and $\beta$ with the electric (3.12) and magnetic (3.15) cases, *i.e.*, $\alpha = \sqrt{D_{\mathrm{e}}/Q_{\mathrm{e}}}$ and $\beta = \sqrt{D_{\mathrm{m}}/Q_{\mathrm{m}}}$ to obtain the bound for combined electric and magnetic dipole radiators:

$$\frac{D}{Q} \leq \left( \sqrt{\frac{D_{\mathrm{e}}}{Q_{\mathrm{e}}}} + \sqrt{\frac{D_{\mathrm{m}}}{Q_{\mathrm{m}}}} \right)^2. \tag{3.23}$$

The combined bound (3.23) is depicted in Fig. 2 for a sphere with polarization $\hat{\boldsymbol{e}} = \hat{\boldsymbol{x}}$. It is seen that $D/Q \leq (1 + \sqrt{1/2})^2 k^3 a^3 \approx 2.9 k^3 a^3$ for this case. For an electrically small, spherical radiator, the bound reads $D/Q \leq 2.9 k_0^3 a^3$. Note that the bound in [8, 9] is sharper than (3.23) for linearly polarized antennas; see also [7] for the circular polarization case.

The upper bound (3.23) requires that the electric and magnetic dipoles contribute equally and have the polarization $\hat{\boldsymbol{e}}$. This gives the partial directivity $D = 3$ and implies that $Q \geq 3/2.9(ka)^{-3}$ for a spherical region. This is similar to the combined TE and TM bound in [17].

# 4 Non Electrically Small Antennas

The general expression (2.8) offers the possibility to analyze $D/Q$ in terms of the current, $\boldsymbol{J}$, that flows on the antenna. It also offers the possibility to optimize an antenna with respect to its $D/Q$ performance. In order to increase the $D/Q$ ratio, we make the assumption that either the stored electric or magnetic energy is greater than the other.

## 4.1 Optimization Formulation for $D/Q$

We illustrate the maximization of (2.8) assuming that the stored electric energy is greater than the stored magnetic energy. Thus, using the amplitude scaling invariance in (2.8), the maximization problem can be reformulated as the following minimization problem:

$$\min_{\boldsymbol{J}} \int_V \int_V \nabla_1 \cdot \boldsymbol{J}(\boldsymbol{r}_1) \nabla_2 \cdot \boldsymbol{J}^*(\boldsymbol{r}_2) \frac{\cos(k|\boldsymbol{r}_1 - \boldsymbol{r}_2|)}{|\boldsymbol{r}_1 - \boldsymbol{r}_2|} - \frac{k}{2}\big(k^2 \boldsymbol{J}_1 \cdot \boldsymbol{J}_2^* - \nabla_1 \cdot \boldsymbol{J}(\boldsymbol{r}_1) \nabla_2 \cdot \boldsymbol{J}^*(\boldsymbol{r}_2)\big) \sin(k|\boldsymbol{r}_1 - \boldsymbol{r}_2|)\, \mathrm{dV}_1\, \mathrm{dV}_2, \quad (4.1)$$

subject to the constraint

$$\left| \int_V \hat{\boldsymbol{e}}^* \cdot \boldsymbol{J}(\boldsymbol{r}) \mathrm{e}^{\mathrm{j}k\hat{\boldsymbol{k}}\cdot\boldsymbol{r}}\, \mathrm{d}V \right| = 1. \quad (4.2)$$

To account for the appropriate class of admissible current densities we also impose the condition

$$\int_V \nabla \cdot \boldsymbol{J}(\boldsymbol{r})\, \mathrm{d}V = 0. \quad (4.3)$$

The first constraint can be reduced to

$$\int_V \hat{\boldsymbol{e}}^* \cdot \boldsymbol{J}(\boldsymbol{r}) \mathrm{e}^{\mathrm{j}k\hat{\boldsymbol{k}}\cdot\boldsymbol{r}}\, \mathrm{d}V = 1, \quad (4.4)$$

using the amplitude scale invariance in (2.8), see Sec. 2.

An alternative technique to the variational method of Sec. 3 for obtaining the optimal currents is described in the following. We represent the current densities in appropriate basis functions $\boldsymbol{\psi}_m$,

$$\boldsymbol{J}(\boldsymbol{r}) = \sum_{m=1}^{M} J_m \boldsymbol{\psi}_m(\boldsymbol{r}), \quad (4.5)$$

and denote $\mathbf{J} = (J_1, J_2, \ldots, J_M)^{\mathrm{T}}$. Introduce the matrix $\mathbf{C}$ with elements

$$C_{mn} = \int_V \int_V \nabla_1 \cdot \boldsymbol{\psi}_m(\boldsymbol{r}_1) \nabla_2 \cdot \boldsymbol{\psi}_n(\boldsymbol{r}_2) \frac{\cos(k|\boldsymbol{r}_1 - \boldsymbol{r}_2|)}{|\boldsymbol{r}_1 - \boldsymbol{r}_2|} - \frac{k}{2}\big(k^2 \boldsymbol{\psi}_m(\boldsymbol{r}_1) \cdot \boldsymbol{\psi}_n(\boldsymbol{r}_2) - \nabla_1 \cdot \boldsymbol{\psi}_m(\boldsymbol{r}_1) \nabla_2 \cdot \boldsymbol{\psi}_n(\boldsymbol{r}_2)\big) \sin(k|\boldsymbol{r}_1 - \boldsymbol{r}_2|)\, \mathrm{dV}_1\, \mathrm{dV}_2 \quad (4.6)$$

for $m, n = 1, 2, ..., M$. The equivalent minimization problem in this basis representation takes the form

$$\min_{J_m} \sum_{m=1}^{M} \sum_{n=1}^{M} J_m^* C_{mn} J_n = \min_{\mathbf{J}} \mathbf{J}^{\mathrm{H}} \mathbf{C} \mathbf{J}, \tag{4.7}$$

subject to the constraints

$$\sum_{m=1}^{M} J_m \int \hat{\boldsymbol{e}}^* \cdot \boldsymbol{\psi}_m(\boldsymbol{r}) \mathrm{e}^{\mathrm{j}k\hat{\boldsymbol{k}}\cdot\boldsymbol{r}} \, \mathrm{d}V = \sum_{m=1}^{M} A_{m,1}^* J_m = 1 \tag{4.8}$$

and

$$\sum_{m=1}^{M} J_m \int \nabla \cdot \boldsymbol{\psi}_m(\boldsymbol{r}) \, \mathrm{d}V = \sum_{m=1}^{M} A_{m,2}^* J_m = 0. \tag{4.9}$$

In matrix notation $\mathbf{A}^{\mathrm{H}}\mathbf{J} = \mathbf{f}$, where: $A_{m,1}^* = \int \hat{\boldsymbol{e}}^* \cdot \boldsymbol{\psi}_m(\boldsymbol{r}) \mathrm{e}^{\mathrm{j}k\hat{\boldsymbol{k}}\cdot\boldsymbol{r}} \, \mathrm{d}V$, $A_{m,2}^* = \int \nabla \cdot \boldsymbol{\psi}_m(\boldsymbol{r}) \, \mathrm{d}V$, and $\mathbf{f} = (1, 0)^{\mathrm{T}}$.

The optimization problem (4.7) to (4.9) is solvable using Lagrange multipliers $\boldsymbol{\nu}$, [15], resulting in the linear system

$$\begin{pmatrix} \mathbf{C} & \mathbf{A} \\ \mathbf{A}^{\mathrm{H}} & \mathbf{0} \end{pmatrix} \begin{pmatrix} \mathbf{J} \\ \boldsymbol{\nu} \end{pmatrix} = \begin{pmatrix} \mathbf{0} \\ \mathbf{f} \end{pmatrix}. \tag{4.10}$$

Note that the constraint (4.9) can be included in the basis functions $\boldsymbol{\psi}_m$. Returning to the matrix $\mathbf{C}$ with elements given in (4.6), note that we can represent the first kernel with cosines as $\mathrm{Re}(G)$ where $G$ is the Green's function corresponding to the scalar Helmholtz equation. Thus, with minor modifications on *e.g.*, a standard method of moments solver, we can implement the above outlined optimization problem. Below we illustrate the solutions of the optimization for planar rectangular structures.

## 4.2 Planar Rectangular Structures

Consider a planar rectangle in the $xz$-plane and broad side radiation $\hat{\boldsymbol{k}} = \hat{\boldsymbol{y}}$ with linear polarization $\hat{\boldsymbol{e}} = \hat{\boldsymbol{x}}$. A Helmholtz decomposition [14] of the current $\boldsymbol{J} = \nabla J^{(\mathrm{g})} + \nabla \times \boldsymbol{J}^{(\mathrm{c})}$ simplifies the corresponding electric energy (2.5) (and equivalently the matrix $\mathbf{C}$ in (4.6)). It is seen that the radiation in the $\hat{\boldsymbol{y}}$-direction is independent of $\boldsymbol{J}^{(\mathrm{c})}$. This reduces the optimization problem (4.10) to the irrotational part of the current density, *i.e.*, we use $\boldsymbol{J}^{(\mathrm{c})} = \mathbf{0}$.

Optimization of the $D/Q$-ratio (2.8) using (4.10) yields the result shown in Fig. 3. The bound is depicted for $k\ell_{\mathrm{x}} = \{0, 0.1, 1, 2, 3\}$ and normalized with the electrical size $k^3a^3$ to decrease the dependence on $ka$, where $a = (\ell_{\mathrm{x}}^2 + \ell_{\mathrm{z}}^2)^{1/2}$. It is observed that it is not possible to distinguish the $k\ell_{\mathrm{x}} = \{0, 0.1, 1\}$ cases in the figure and that the bound increases slightly for the $k\ell_{\mathrm{x}} = \{2, 3\}$ cases. The results for $k\ell_{\mathrm{x}} = \{2, 3\}$ are only shown when their corresponding $Q$-factors are sufficiently large, see the corresponding $Q$-values in Fig. 3. This means that there are no severe bounds on $Q$ for these rather large structures. Note that $ka \approx 10$ for $k\ell_{\mathrm{x}} = 2$ and $\ell_{\mathrm{z}}/\ell_{\mathrm{x}} = 20$. The figures also contain the asymptotic expressions based on (C.5) where it is assumed that the current is of the form $\boldsymbol{J} = J_{\mathrm{x}}(x)\hat{\boldsymbol{x}}$ and $k\ell_{\mathrm{z}} \gg 1$.

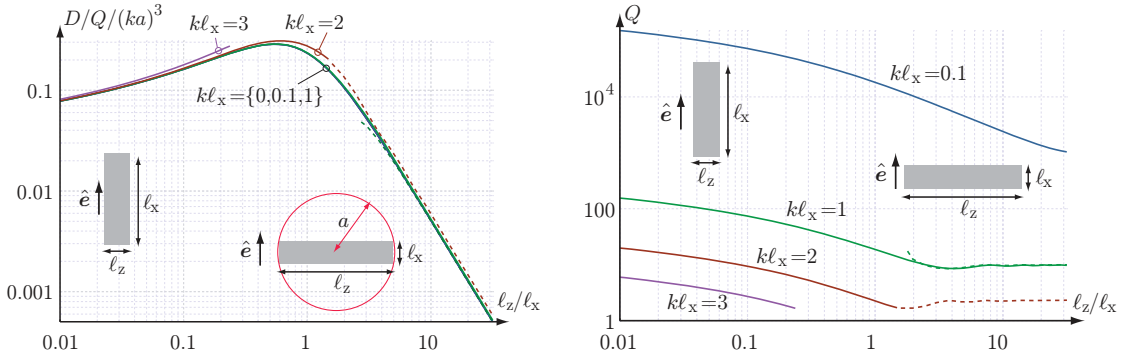


**Figure 3**: (left) Bound on $D/Q$ for a planar rectangle with sides $\ell_x$ and $\ell_z$ for $k\ell_x = \{0, 0.1, 1, 2, 3\}$ and $\hat{\boldsymbol{k}} = \hat{\boldsymbol{y}}$ normal to the rectangle and $\hat{\boldsymbol{e}} = \hat{\boldsymbol{x}}$. The solid curves show the bounds determined for irrotational currents, $\nabla \times \boldsymbol{J} = \boldsymbol{0}$, using (4.10). The dashed curves shows the corresponding asymptotic results using (C.5). (right) Resulting $Q$ factors.

# 5 Negative Electric Energy

In the previous section, Sec. 4.2, we removed the loop-currents $\boldsymbol{J}^{(c)}$ through the observation that they do not contribute to the radiation in the normal direction. If the numerical optimization is done with these currents, it is observed that they may cause a negative stored electric energy (2.5). This behavior of the stored electric energy is illustrated here using simple examples.

Consider first the following divergence free *i.e.*, $\nabla \cdot \boldsymbol{J} = 0$, current density $\boldsymbol{J}(\boldsymbol{r}) = I_0 \delta(\varrho - a)\delta(z)\hat{\boldsymbol{\phi}}$, where $\delta$ denotes the Dirac delta distribution, $I_0$ is a constant that depends on the source of current, and the cylindrical coordinates $(\varrho, \phi, z)$ are used. In this case, the stored electric energy (2.5) reduces to

$$w^{(e)} = -\pi k^3 a^2 I_0^2 \int_0^{2\pi} \cos\phi \sin\left(2ka \sin\frac{\phi}{2}\right) \mathrm{d}\phi. \tag{5.1}$$

Numerical integration shows that $w^{(e)}$ is positive for $ka < 1.5$, see Fig. 4. When the electric size of the structure increases, the electric energy becomes negative for some objects. It is noted that the corresponding stored magnetic energy is infinite for the considered current.

For a rectangular surface of dimensions $\ell_x, \ell_y$ we use the current density $\boldsymbol{J} = I_0 \delta(z)\big((\delta(y+\ell_y/2) - \delta(y-\ell_y/2))\hat{\boldsymbol{x}} + (\delta(x-\ell_x/2) - \delta(x+\ell_x/2))\hat{\boldsymbol{y}}\big)$. The corresponding electrical energy is shown in Fig. 4.

For a thin circular annulus of radius $a$ and width $\Delta$ we consider a current density of the form $\boldsymbol{J} = -I_0 \delta(z)\hat{\boldsymbol{\phi}}/\Delta$ for $a - \Delta \leq \varrho \leq a$ and zero otherwise, using cylindrical coordinates. The integrals are evaluated using the singularity cancellation methods, see Fig. 4. It is seen here that for small values of $k$, the stored energy is predominantly magnetic. When $k$ increases, the two stored energies appear to equalize.

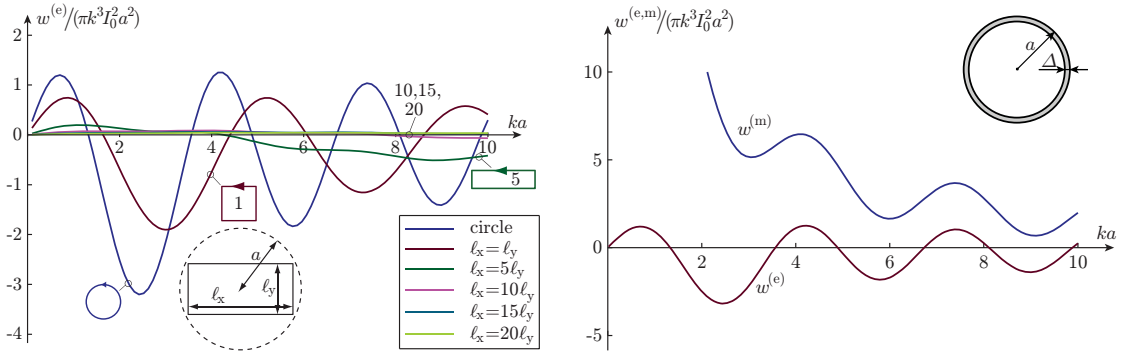


**Figure 4**: (left) Stored electric energy for circular (5.1) and rectangular loop currents. (right) Stored electric and magnetic energies for circular currents with width $\Delta = 0.005a$.

# 6 Numerical examples

We illustrate the theoretical results with numerical examples of the current distributions on spherical regions, current distributions and bounds on strip dipoles, and planar rectangular array antennas.

## 6.1 Spherical Region

It is observed that the currents that generate the optimal $D/Q$-ratios are not unique. We illustrate this for a simple electric case, in the limit of small $ka$ so that we can use the variational formulation in (3.5). Consider a spherical volume with radius $a$ and electric polarization $\hat{\boldsymbol{e}} = \hat{\boldsymbol{z}}$. The optimal charge distribution determined from (3.11) is of the form $\rho(\theta,\phi) = \rho_0 \cos\theta$. The corresponding current density satisfies $\nabla \cdot \boldsymbol{J} = -\mathrm{j}k\rho$ (recall $\rho_{\mathrm{SI}} = \rho/c_0$) on the surface of the sphere. This gives

$$\frac{\partial}{\partial\theta}\big(\sin\theta J_\theta\big) + \frac{\partial J_\phi}{\partial\phi} = \frac{-\mathrm{j}ka\rho_0\sin(2\theta)}{2} \tag{6.1}$$

This equation has many solutions, *e.g.*, all the functions of the form

$$\boldsymbol{J} = J_{\theta 0}\hat{\boldsymbol{\theta}}\big(\sin\theta - \frac{\beta}{\sin\theta}\big) + \frac{1}{\sin\theta}\frac{\partial A}{\partial\phi}\hat{\boldsymbol{\theta}} - \frac{\partial A}{\partial\theta}\hat{\boldsymbol{\phi}} \tag{6.2}$$

where $J_{\theta 0} = -\mathrm{j}ka\rho_0$, $\beta$ is a constant, and $A = A(\theta,\phi)$.

The simplest solution to (6.1) is a rotationally symmetric current density in the $\hat{\boldsymbol{\theta}}$-direction that vanishes as $\theta = 0$ and $\theta = \pi$, *i.e.*, $\boldsymbol{J} = \hat{\boldsymbol{\theta}} J_{\theta 0}\sin\theta$. This is a current density that generates a single spherical TM mode. It is noted that the current density on a folded spherical dipole has this form, see Fig. 5a. An alternative solution is obtained by the requirement that the current density vanishes at $\theta = \pi/2$. This gives the solution $\boldsymbol{J} = J_{\theta 0}\hat{\boldsymbol{\theta}}(\sin\theta - 1/\sin\theta)$, see Fig. 5b. This current density is infinite at $\theta = 0$ and $\theta = \pi$ and resembles the current density on a capped spherical dipole [16]. A third solution is offered by $\beta = 0$ and $A = A(\theta)$. In particular,

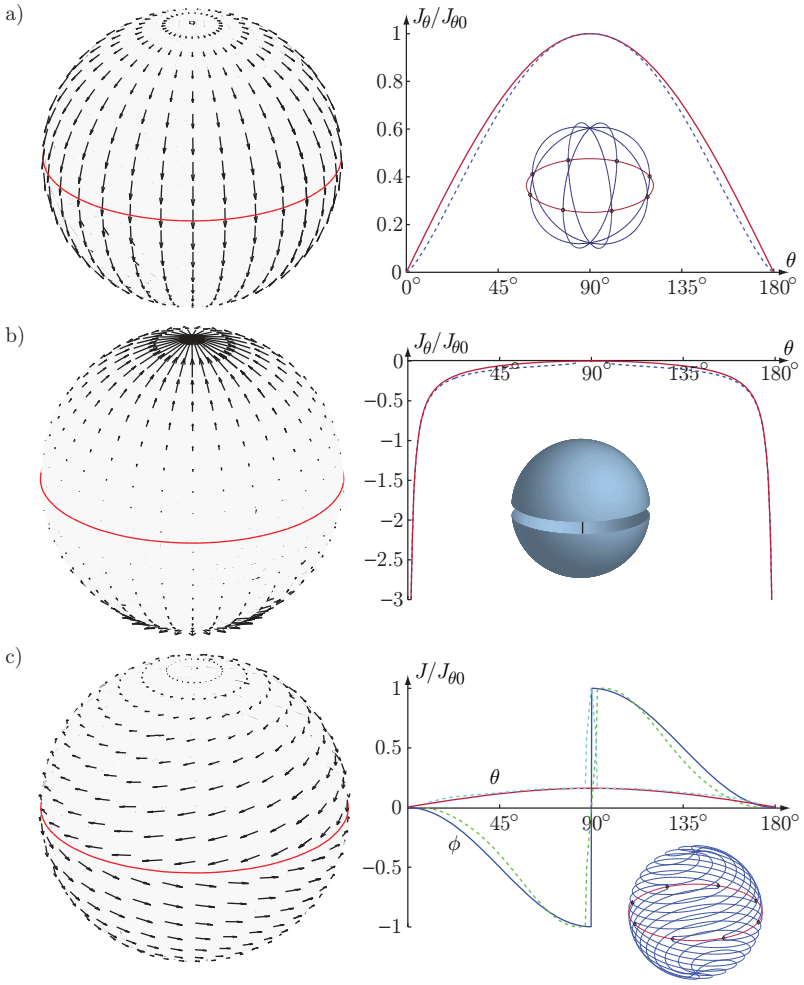


**Figure 5**: Examples of current distributions on spheres with the charge density $\rho = \rho_0 \cos\theta$. a) folded spherical dipole with $\boldsymbol{J} \approx J_{\theta 0}\hat{\boldsymbol{\theta}} \sin\theta$. b) capped spherical dipole with $\boldsymbol{J} \approx J_{\theta 0}\hat{\boldsymbol{\theta}}(\sin\theta - 1/\sin\theta)$. c) folded spherical helix with $\boldsymbol{J} \approx J_{\theta 0}\big(0.15\hat{\boldsymbol{\theta}} \sin\theta - \hat{\boldsymbol{\phi}} \operatorname{sign}(\cos\theta) \sin^2\theta\big)$.

we consider the current density $\boldsymbol{J} = J_{\theta 0}\big(0.15\hat{\boldsymbol{\theta}} \sin\theta - \hat{\boldsymbol{\phi}} \operatorname{sign}(\cos\theta) \sin^2\theta\big)$, as this solution is similar to the current density on a spherical folded helix, see Fig. 5c.

## 6.2 Strip Dipole Antennas

The optimal current distributions are determined for rectangles with side lengths $\ell_y = \xi \ell_x$ with $\xi = \{0.1, 0.01, 0.001\}$ using (4.10) for $ka \leq 2$. The current in the center $\boldsymbol{J}(x, 0) = J_x(x)\hat{\boldsymbol{x}}$ is depicted in Fig. 6 for the half-wave antenna, *i.e.*, $ka \approx 1.5$, where $a = (\ell_x^2 + \ell_y^2)^{1/2}/2$. It is observed that the currents resemble the commonly assumed $\cos(\pi x/\ell_x)$ shape.

The corresponding bound on $D/Q$ normalized with $(ka)^3$ is shown in Fig. 7. Here it is seen that the performance improves with the width of the rectangle. Moreover,

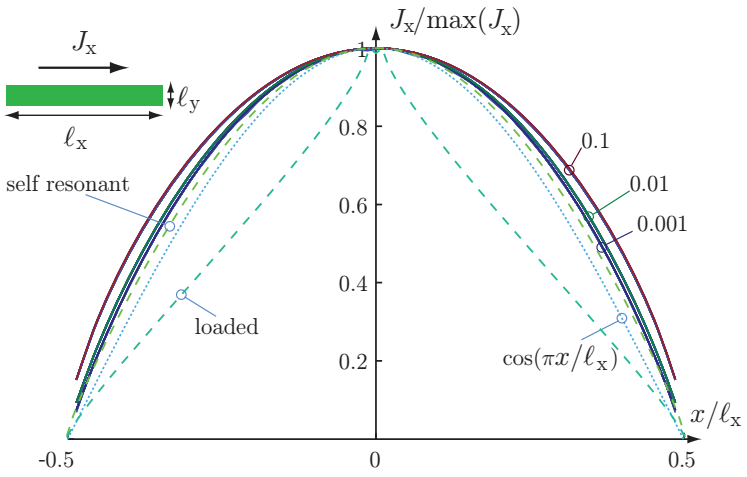


**Figure 6**: Optimal current distribution (4.10) for planar rectangles with side lengths $\ell_y = \xi\ell_x$ with $\xi = \{0.1, 0.01, 0.001\}$ and $ka = 1.5$ (solid curves). Simulated currents on a strip dipole for the inductively loaded and the self-resonant and case respectively with $\ell_y = 0.01\ell_x$ for $ka \approx \{0.28, 1.49\}$ (dashed curves). Theoretical current distribution, $\cos(\pi x/\ell_x)$(dotted curve)

$D/(Qk^3a^3)$ is nearly independent of the electrical size of the structure for $ka \leq 1.5$.

The resulting Q-factor is computed from the current distribution using the radiated power in [19], see Fig. 8. It is observed that $Q$ decreases with the increase of the width of the strip. The directivity $D$ is depicted in Fig. 8. Here, it is seen that the directivity increases with the electrical size of the object.

The bounds are compared with numerical results for a center fed strip dipole with $\ell_y = 0.01\ell_x$. The dipole is self-resonant for $ka \approx 1.49$ with the directivity $D \approx 1.63$. The Q-factor is estimated to $Q \approx 6$ using the differentiation of the impedance [11, 24]. These results are indicated with stars at $ka \approx 1.49$ in Figs 7 to 8. The corresponding current density is also depicted in Fig. 6. It is observed that the self-resonant dipole has a current distribution that resembles the optimal current distribution. The estimated values of $D/Q$, $D$, and $Q$ are also close the corresponding optimal values.

It is also illustrative to consider an inductively loaded strip dipole with the same dimensions. The loading decreases the resonance wavenumber to $ka \approx 0.28$ and the parameters are estimated to $D \approx 1.5$, $Q \approx 1250$, and $D/(Qk^3a^3) \approx 0.054$, see the stars at $ka \approx 0.28$ in Figs 7 to 8. It is observed that the performance of the loaded dipole is farther away from the optimum than the performance of the unloaded dipole. This is also seen from the shape of the current distribution in Fig. 6.

## 6.3 Array Antennas

The performances of linear arrays are illustrated with numerical results using the method of moments (MoM) for dipole and capacitively loaded dipole elements. The one-dimensional dipole array consists of $n$ elements with the length $\ell_x$ and the width

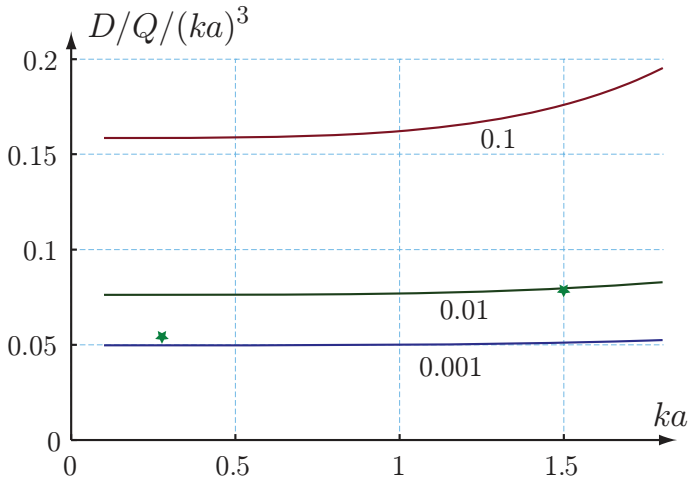


**Figure 7**: Bound on $D/Q$ normalized with $k^3a^3$ for a planar rectangle with side lengths $\ell_y = \xi\ell_x$ where $\xi = \{0.1, 0.01, 0.001\}$. The numerical results for strip dipoles with $\xi = 0.01$ and $ka \approx \{0.28, 1.49\}$ are indicated by the stars.

$\Delta = \ell_x/50$ and inter-element spacing $\ell_x$. This gives approximately arrays with half a wavelength, $\lambda_0/2$, spacing. The array is modeled as perfectly conducting with a gap feed model. The passive array is analyzed, where identical lumped resistances, $R_0$, are placed in the feed gaps. The resistance $R_0$ is determined by maximizing the effective antenna aperture at the first resonance frequency, see [12] for details.

The dipole array is compared with the physical bounds for antennas confined to rectangular regions, see Fig. 3. The electric polarization of the arrays is aligned with the $\ell_x$-direction. The arrays with $n$ elements are circumscribed by rectangles with height $\ell_x$ and width $\ell_z = (n-1)\ell_x + \ell_x/50$ for $n = 1, ..., 10$. The corresponding results are shown in Fig. 9, where the effective antenna aperture is normalized with the physical area, $A$. The physical bound is drawn for $k\ell_x = 0$ and the asymptotic result in App. C for $k\ell_x = \{1, 2\}$. It is observed that the performances of the capacitively loaded dipoles are close to the physical bound. The dipole array is a factor of 1/15 below the physical bound. Using the polarization interpretation on the array of [12] we see that this is due to the reduction of polarizability of the dipole as compared with the rectangle.

# 7 Conclusions

Upper bounds on the directivity antenna $Q$ quotient, $D/Q$, are derived based on a quadratic optimization problem. The $D/Q$ quotient is formulated in the current density on the antenna structure as given from the radiation intensity and the expressions of the stored energies in [5, 19, 20]. The expression is not bases on a small antenna limit assumption opening the possibility to analyze electrically large structures. The optimization problem is solved analytically in the limit of small antennas and numerically using Lagrange parameters for arbitrary size antennas. The upper

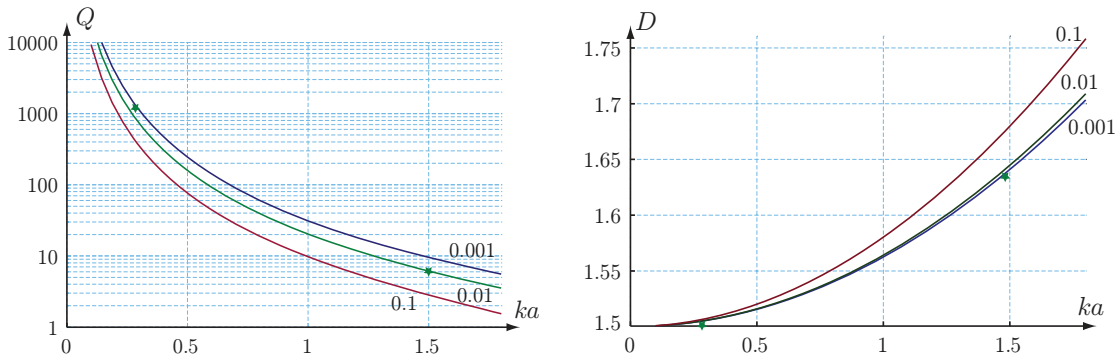


**Figure 8**: $Q$ factor (left) and directivity (right) for the optimal current distributions corresponding to the $D/Q$ bound in Fig. 7. The numerical results for strip dipoles with $\xi = 0.01$ and $ka \approx \{0.28, 1.49\}$ are indicated by the stars.

bounds are useful as they show how the shape and size of the antenna geometry affect the antenna performance [6, 8, 9]. They can also be used as a priori estimates of what can be expected from an antenna in a given geometry.

The closed form solution for small antennas expresses the bounds in the polarizability of the antenna structure. The bound on non-magnetic antenna structures is identical to the bound in [6, 8, 9] and agrees with the results in [23] for the directivity $D = 3/2$. In [20], Vandenbosch considered the corresponding bound on $Q$ for small antennas using a line search optimization algorithm. In contrast, the results presented here are for $D/Q$ where the bound can be solved analytically. This formulation distinguishes between the polarizations (linear, in different directions as well as circular). It is also shown that it is sufficient to consider surface currents in this small $ka$-limit. Moreover, the case with combined electric and magnetic dipoles is analyzed, where it is noted that the results resemble the mixed TE and TM bound in [17] for spherical regions.

We also illustrate that there are several current densities for a given charge density. The explicit solutions for a spherical region include current distributions that resemble the current on folded spherical dipoles, capped spherical dipoles, and folded spherical helices.

Lagrange multipliers are used to solve the $D/Q$ optimization problem for finite size antennas. This reformulates the problem of obtaining the optimal current densities as a linear system that has many similarities with standard method of moments solvers. It is shown that the bound performs well for fairly large antennas with high directivity. It is illustrated that the stored electric energy in [19] can be negative for certain kinds of loop type currents on planar structures. Although this stored energy corresponds to a case that can cause numerical problems this can be mitigated with a Helmholtz decomposition of the current density.

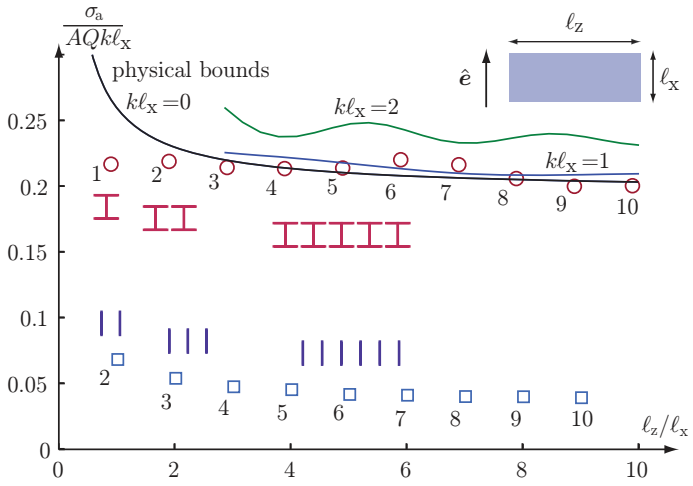


**Figure 9**: Illustrations of the physical bounds on the absorption cross section planar rectangular circumscribing regions with height $\ell_x$, width $\ell_z$, and physical area $A = \ell_x\ell_z$.


# Acknowledgments

This work was supported in part by Swedish Research Council (VR) and the Swedish Governmental Agency for Innovation Systems (IMT-advanced and beyond and the VINN Excellence Center Chase).


# Appendix A Small Antenna Decoupling

The maximization problem (3.4) decouples into two separate problems, one for $\rho \neq 0, \boldsymbol{J} = \boldsymbol{0}$ and one for $\boldsymbol{J} \neq \boldsymbol{0}, \rho = 0$ corresponding to antennas radiating as an electric dipole and as a magnetic dipole, respectively. The key to this decoupling is the independent maximization of $\rho$ and $\boldsymbol{J}$ in (3.4). A contradiction argument shows that the two energy terms of the denominator have to be equal for the maximizing $\rho, \boldsymbol{J}$. This reduces the problem to a constrained quadratic maximization problem. The constraints on charge and current densities are included with the method of Lagrange parameters. The resulting Euler-Lagrange equations reduce the equations (3.10) and (3.19), *e.g.*, to the solutions of the two separate optimization problems. A similar problem for vectors or scalars is stated in (3.22), and the above outlined method yields the desired result.

# Appendix B Integral Equations for BoR

Consider a body of revolution (BoR) with $\hat{\boldsymbol{z}}$ as the axis of revolution [1], see Fig. 10. The object is parameterized by the curve $\{\varrho(\ell), z(\ell)\}$ for $\ell \in [\ell_a, \ell_b]$, where $\varrho = \sqrt{x^2 + y^2}$. The electric high contrast polarizability dyadic can be written as $\boldsymbol{\gamma}_\infty =$

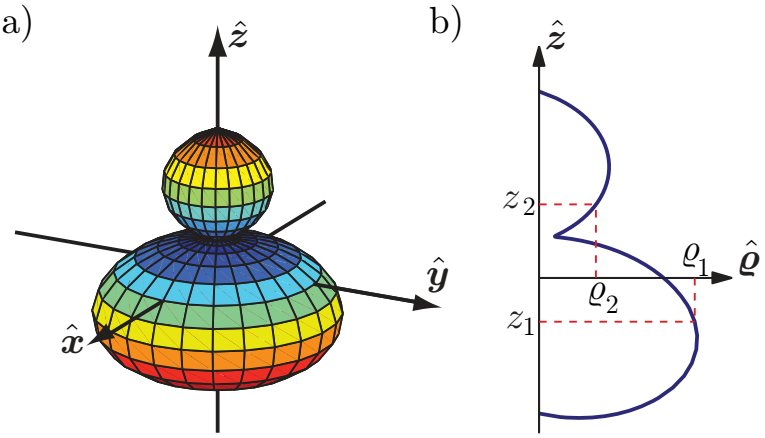


**Figure 10**: Illustration of a body of revolution (BoR) object.

$\gamma_{\mathrm{h}}(\hat{\boldsymbol{x}}\hat{\boldsymbol{x}}+\hat{\boldsymbol{y}}\hat{\boldsymbol{y}})+\gamma_{\mathrm{v}}\hat{\boldsymbol{z}}\hat{\boldsymbol{z}}$, where $\gamma_{\mathrm{h}}$ and $\gamma_{\mathrm{v}}$ are the polarizabilities for horizontal ($\hat{\boldsymbol{e}}\cdot\hat{\boldsymbol{z}}=0$) and vertical ($\hat{\boldsymbol{e}}=\hat{\boldsymbol{z}}$) polarizations, respectively. Here, we restrict the analysis to horizontal polarization for simplicity, see also [10].

For the electric dipole in Sec. 3.1, a Fourier series ansatz gives the surface charge density $\rho_{\mathrm{s}}(\boldsymbol{r}) = \rho_{\mathrm{s}\ell}(\ell)\cos\phi$ and the right-hand side of (3.11) becomes $E_0\varrho\cos\phi$, where $\hat{\boldsymbol{e}}=\hat{\boldsymbol{x}}$ is used. This simplifies the integral equation (3.11) to

$$\int_{\ell_{\mathrm{a}}}^{\ell_{\mathrm{b}}} \rho_{\mathrm{s}\ell}(\ell_1) g_1(\ell_1,\ell_2)\varrho(\ell_1)\left|\frac{\partial \boldsymbol{r}_1}{\partial \ell_1}\right| \mathrm{d}\ell_1 = 2\pi E_0 \varrho(\ell_2), \tag{B.1}$$

where $g_1 = \int_0^\pi \frac{\cos\phi}{R}\,\mathrm{d}\phi$ is the modal Green's function, $R=(\varrho_1^2+\varrho_2^2-2\varrho_1\varrho_2\cos\phi+(z_1-z_2)^2)^{1/2}$, and $|\partial\boldsymbol{r}_1/\partial\ell_1|$ is the Jacobian. Solve for $\rho_{\mathrm{s}\ell}$ and determine the polarizability

$$\gamma = \frac{1}{E_0}\int_{\partial V} \hat{\boldsymbol{e}}\cdot\boldsymbol{r}\rho_{\mathrm{s}\ell}(\boldsymbol{r})\,\mathrm{dS} = \frac{\pi}{E_0}\int \varrho^2\rho_{\mathrm{s}\ell}(\ell)\left|\frac{\partial\boldsymbol{r}}{\partial\ell}\right|\mathrm{d}\ell. \tag{B.2}$$

For the magnetic dipole case in Sec. 3.2 we consider $\hat{\boldsymbol{h}}=\hat{\boldsymbol{z}}$ and currents $\boldsymbol{J} = J_\phi(\ell)\hat{\boldsymbol{\phi}}$. The integral equation simplifies to

$$\int_{\ell_a}^{\ell_b}\int_0^{2\pi} \frac{\hat{\boldsymbol{\phi}}_2\cdot\hat{\boldsymbol{\phi}}_1 J_\phi(\ell_1)}{4\pi|\boldsymbol{r}_1-\boldsymbol{r}_2|}\varrho(\ell_1)\left|\frac{\partial\boldsymbol{r}_1}{\partial\ell_1}\right|\mathrm{d}\phi_1\,\mathrm{d}\ell_1 = \frac{H_0}{2}\hat{\boldsymbol{\phi}}_2\cdot\hat{\boldsymbol{h}}\times\boldsymbol{r}_2 \tag{B.3}$$

for $\boldsymbol{r}_2\in\partial V$. This can be written as

$$\int_{\ell_a}^{\ell_b} J_\phi(\ell_1)g_1(\ell_1,\ell_2)\varrho(\ell_1)\left|\frac{\partial\boldsymbol{r}_1}{\partial\ell_1}\right|\mathrm{d}\ell_1 = \pi H_0\varrho(\ell_2) \tag{B.4}$$

for $\hat{\boldsymbol{h}}=\hat{\boldsymbol{z}}$. Solve for $J_\phi$ and compute

$$\nu = \frac{1}{2H_0}\int_{\partial V}\hat{\boldsymbol{z}}\times\boldsymbol{r}\cdot J_\phi\hat{\boldsymbol{\phi}}\,\mathrm{dS} = \frac{\pi}{H_0}\int_{\ell_a}^{\ell_b} J_\phi\varrho^2\left|\frac{\partial\boldsymbol{r}}{\partial\ell}\right|\mathrm{d}\ell. \tag{B.5}$$

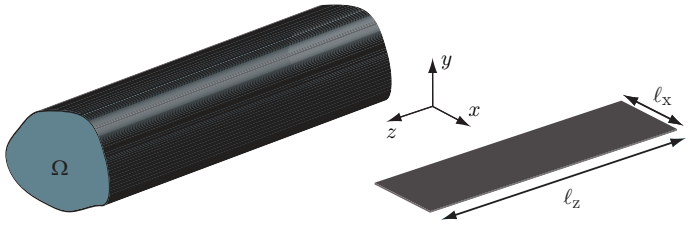


**Figure 11**: Elongated objects with length $\ell = \ell_z$ and cross section $\Omega$ in the $xy$-plane.

We note that the integral equations for the charge density and the azimuthal current density are formally identical except for a factor of 2 in the right hand side of (B.1) as compared with the (B.4). The expressions for $\gamma$ and $\nu$ are also identical. This implies that $\nu = \gamma/2$, *i.e.*, the bound for the magnetic dipole radiation is 1/2 of the corresponding electric case for BoR objects with horizontal polarization.

# Appendix C Elongated Objects

The bound in [8, 9] shows that $D/Q$ is bounded by the projection of the polarization on the polarizability dyadic. It is observed that the polarizability is large for directions parallel with the longest dimension of *e.g.*, spheroids, cylinders, and rectangles [8, 9]. The polarizability is often much lower for directions perpendicular to the longest dimension.

Consider an elongated object $V = \Omega \times [-\ell/2, \ell/2]$ with $k\ell \gg 1$, and the longest dimension contained in the $xz$-plane, see Fig. 11. The optimization formulation (4.1) can be used for arbitrary directions $\hat{\boldsymbol{k}}$ and polarizations $\hat{\boldsymbol{e}}$. Here, we analyze the case with broadside radiation, *i.e.*, $\hat{\boldsymbol{k}} \cdot \hat{\boldsymbol{z}} = 0$ and polarization $\hat{\boldsymbol{e}} \cdot \hat{\boldsymbol{z}} = 0$. It is assumed that the current is independent of the $z$-coordinate. This gives the stored electric energy $\widetilde{W}^{(\mathrm{e})}_{\mathrm{vac}} = \frac{\mu_0 \ell}{16\pi k^2} \tilde{w}^{(\mathrm{e})}$, with

$$\tilde{w}^{(\mathrm{e})}(\boldsymbol{J}) = \int_\Omega\int_\Omega \nabla_1 \cdot \boldsymbol{J}(\boldsymbol{\varrho}_1)\nabla_2 \cdot \boldsymbol{J}^*(\boldsymbol{\varrho}_2) G_1(k|\boldsymbol{\varrho}_1 - \boldsymbol{\varrho}_2|, k\ell)$$
$$- \frac{k\ell}{2}\left(k^2 \boldsymbol{J}(\boldsymbol{\varrho}_1)\cdot\boldsymbol{J}^*(\boldsymbol{\varrho}_2) - \nabla_1 \cdot \boldsymbol{J}(\boldsymbol{\varrho}_1)\nabla_2 \cdot \boldsymbol{J}^*(\boldsymbol{\varrho}_2)\right) G_2(k|\boldsymbol{\varrho}_1 - \boldsymbol{\varrho}_2|, k\ell)\,\mathrm{dS}_1\mathrm{dS}_2. \quad \text{(C.1)}$$

Here we use the notation $\boldsymbol{\varrho}_n$, $n = 1, 2$ to account for vectors in the $xy$-plane, and $\varrho = |\boldsymbol{\varrho}|$. The two integral kernels $G_1$, $G_2$ have their $z$-dependence integrated out asymptotically for large $k\ell$:

$$G_1(k\varrho, k\ell) = \frac{1}{\ell}\int_{\frac{-\ell}{2}}^{\frac{\ell}{2}}\int_{\frac{-\ell}{2}}^{\frac{\ell}{2}} \frac{\cos\left(k\sqrt{\varrho^2 + (z_1 - z_2)^2}\right)}{\sqrt{\varrho^2 + (z_1 - z_2)^2}}\,\mathrm{d}z_1\mathrm{d}z_2$$
$$= -\pi \mathrm{N}_0(k\varrho) + 2\frac{\sin(k\varrho)}{k\ell} - 2\frac{\sqrt{1 + \varrho^2/\ell^2}}{k^2\ell^2}\cos\left(k\sqrt{\ell^2 + \varrho^2}\right) + \mathcal{O}((k\ell)^{-3}), \quad \text{(C.2)}$$

and

$$G_2(k\varrho, k\ell) = \frac{1}{\ell^2}\int_{\frac{-\ell}{2}}^{\frac{\ell}{2}}\int_{\frac{-\ell}{2}}^{\frac{\ell}{2}} \sin\Big(k\sqrt{\varrho^2+(z_1-z_2)^2}\Big)\,\mathrm{d}z_1\mathrm{d}z_2$$
$$= -\frac{\pi\varrho}{\ell}\mathrm{N}_1(k\varrho) - 2\frac{\varrho^2/\ell^2+1}{k^2\ell^2}\sin(k\ell\sqrt{1+\varrho^2/\ell^2})$$
$$- \frac{2\varrho}{k\ell^2}\cos(k\varrho) + \frac{2}{k^2\ell^2}\sin(k\varrho) + \mathcal{O}((k\ell)^{-3}), \quad \text{(C.3)}$$

where $\mathrm{N}_n$ is the Neumann function of order $n$. The corresponding radiated power in a direction orthogonal to the $z$-axis, $\hat{\boldsymbol{k}}\cdot\hat{\boldsymbol{z}} = 0$, with polarization $\hat{\boldsymbol{e}}\cdot\hat{\boldsymbol{z}} = 0$ is

$$P(\hat{\boldsymbol{k}}, \hat{\boldsymbol{e}}) = \frac{\zeta_0\ell^2k^2}{32\pi^2}\left|\int_\Omega \hat{\boldsymbol{e}}\cdot\boldsymbol{J}(\boldsymbol{\varrho})\mathrm{e}^{\mathrm{j}k\hat{\boldsymbol{k}}\cdot\boldsymbol{\varrho}}\,\mathrm{dS}\right|^2. \quad \text{(C.4)}$$

This gives the bound

$$\frac{D}{Q} \le \max_{\boldsymbol{J}} \frac{k^3\ell\left|\int_\Omega \hat{\boldsymbol{e}}\cdot\boldsymbol{J}(\boldsymbol{\varrho})\mathrm{e}^{\mathrm{j}k\hat{\boldsymbol{k}}\cdot\boldsymbol{\varrho}}\,\mathrm{dS}\right|^2}{\tilde{w}^{(\mathrm{e})}(\boldsymbol{J})}, \quad \text{(C.5)}$$

for currents $\boldsymbol{J} = \boldsymbol{J}(\boldsymbol{\varrho})$.

# References


[1] M. Andreasen. Scattering from bodies of revolution. *IEEE Trans. Antennas Propagat.*, **13**(2), 303–310, 1965.

[2] Antenna Standards Committee of the IEEE Antennas and Propagation Society. IEEE Standard Definitions of Terms for Antennas, 1993. IEEE Std 145-1993.

[3] S. R. Best. Low Q electrically small linear and elliptical polarized spherical dipole antennas. *IEEE Trans. Antennas Propagat.*, **53**(3), 1047–1053, 2005.

[4] L. J. Chu. Physical limitations of omni-directional antennas. *Appl. Phys.*, **19**, 1163–1175, 1948.

[5] W. Geyi. A method for the evaluation of small antenna Q. *IEEE Trans. Antennas Propagat.*, **51**(8), 2124–2129, 2003.

[6] M. Gustafsson, M. Cismasu, and S. Nordebo. Absorption efficiency and physical bounds on antennas. *International Journal of Antennas and Propagation*, (Article ID 946746), 1–7, 2010.

[7] M. Gustafsson and C. Sohl. New physical bounds on elliptically polarized antennas. In *Proceedings of the Third European Conference on Antennas and Propagation*, pages 400–402, Berlin, Germany, March 23–27 2009. The Institution of Engineering and Technology.

[8] M. Gustafsson, C. Sohl, and G. Kristensson. Physical limitations on antennas of arbitrary shape. *Proc. R. Soc. A*, **463**, 2589–2607, 2007.

[9] M. Gustafsson, C. Sohl, and G. Kristensson. Illustrations of new physical bounds on linearly polarized antennas. *IEEE Trans. Antennas Propagat.*, **57**(5), 1319–1327, May 2009.

[10] M. Gustafsson. Polarizability and physical bounds on antennas in cylindrical and rectangular geometries. Technical Report LUTEDX/(TEAT-7195)/1-11/(2010), Lund University, Department of Electrical and Information Technology, P.O. Box 118, S-221 00 Lund, Sweden, 2010. `http://www.eit.lth.se`.

[11] M. Gustafsson and S. Nordebo. Bandwidth, Q factor, and resonance models of antennas. *Progress in Electromagnetics Research*, **62**, 1–20, 2006.

[12] B. L. G. Jonsson and M. Gustafsson. Limitations on the effective area and bandwidth product for array antennas. In *Proc. URSI Int Electromagnetic Theory (EMTS) Symp*, pages 711–714, 2010.

[13] R. E. Kleinman and T. B. A. Senior. Rayleigh scattering. In V. V. Varadan and V. K. Varadan, editors, *Low and high frequency asymptotics*, volume 2 of *Handbook on Acoustic, Electromagnetic and Elastic Wave Scattering*, chapter 1, pages 1–70. Elsevier Science Publishers, Amsterdam, 1986.

[14] M. Mitrea. Sharp Hodge decompositions, Maxwell's equations, and vector Poisson problems on nonsmooth, three-dimensional Riemannian manifolds. *Duke Mathematical Journal*, **125**(3), 467–547, 2004.

[15] G. Strang. *Introduction to applied mathematics*. Wellesley-Cambridge Press, Box 157, Wellesley MA 02181, 1986.

[16] H. R. Stuart. Eigenmode analysis of a two element segmented capped monopole antenna. *IEEE Trans. Antennas Propagat.*, **57**(10), 2980–2988, 2009.

[17] H. L. Thal. New radiation Q limits for spherical wire antennas. *IEEE Trans. Antennas Propagat.*, **54**(10), 2757–2763, October 2006.

[18] J. van Bladel. *Electromagnetic Fields*. IEEE Press, Piscataway, NJ, second edition, 2007.

[19] G. A. E. Vandenbosch. Reactive energies, impedance, and Q factor of radiating structures. *IEEE Trans. Antennas Propagat.*, **58**(4), 1112–1127, 2010.

[20] G. A. E. Vandenbosch. Simple procedure to derive lower bounds for radiation Q of electrically small devices of arbitrary topology. *Antennas and Propagation, IEEE Transactions on*, **59**(6), 2217–2225, 2011.

[21] J. Volakis, C. C. Chen, and K. Fujimoto. *Small Antennas: Miniaturization Techniques & Applications*. McGraw-Hill, New York, 2010.

[22] A. D. Yaghjian. Internal energy, Q-energy, Poynting's theorem, and the stress dyadic in dispersive material. *IEEE Trans. Antennas Propagat.*, **55**(6), 1495–1505, 2007.

[23] A. D. Yaghjian and H. R. Stuart. Lower bounds on the Q of electrically small dipole antennas. *IEEE Trans. Antennas Propagat.*, **58**(10), 3114–3121, 2010.

[24] A. D. Yaghjian and S. R. Best. Impedance, bandwidth, and $Q$ of antennas. *IEEE Trans. Antennas Propagat.*, **53**(4), 1298–1324, 2005.